Off-shell properties of the two-nucleon t matrix

K. Amos, L. Berge, F. A. Brieva,* A. Katsogiannis, L. Petris, and L. Rikus†
School of Physics, University of Melbourne, Parkville, Victoria, Australia 3052
(Received 5 May 1987)

The off-shell properties of two-nucleon t matrices are studied for both uncoupled and coupled channels. Complex t matrices have been obtained using both matrix inversion and continued fraction techniques of solution and predicated upon a standard phenomenological form (Reid), a meson exchange model (Paris), and a new phenomenological form that we have developed, of the two-nucleon interaction. The off-shell t matrices from these interactions are very similar whenever they give essentially the same phase shifts at all energies. When they do not, the associated off-shell t matrices diverge so substantially that any data depending upon these off-shell t matrices will differentiate between the interactions.

I. INTRODUCTION

Knowledge of the off-shell properties of the two nucleon t matrix is necessary whenever a detailed microscopic description of a nuclear system is sought. This requirement has been realized both in the calculation of few and of many-nucleon systems. In the last few years, the importance of the off-shell behavior of the nucleon-nucleon t matrix has also become apparent in the microscopic description of nucleon scattering from nuclei, determining the properties of both the nucleon self-energy and the effective interaction responsible for the nuclear transitions and nuclear rearrangement processes.

The scattering of nucleon off nuclei provide an interesting situation to probe the t matrix fully off of the energy shell.[1] Indeed, a simple model for calculating the nucleon-nucleus optical potential requires the t matrix between the projectile and each and every bound nucleon in the target nucleus, the interaction then clearly taking place well off of the energy shell. However, the difficulties found in explicitly calculating the off-shell behavior of the t matrix, further complicated when medium corrections are accounted for have led many authors to construct effective forces which reproduce the on-shell t matrix but neglect its off-shell properties. However some off-shell components may be simulated by adequate averages leading to a density and energy dependent effective force.[2] This is the case, for example, of an energy and density dependent effective interaction[3] built upon the Paris internucleon force[4] and which has been used with reasonable success for distorted wave approximation studies of inelastic proton scattering.[5]

Our approach to the calculation of the t-matrix off-shell behavior is a nonrelativistic one, namely we assume the existence of a well determined nucleon-nucleon potential and then the off-shell properties are given by the solution of the corresponding Lippman-Schwinger equation of the t matrix. However, the existence of several phase-shift equivalent internucleon forces makes uncertain the determination of the off-shell t matrix. It is important therefore to understand what are the differences in the off-shell properties of the t matrix as calculated from different internucleon forces before one can estimate their effects in many-nucleon calculations.

In this paper we address ourselves firstly to the problem of specifying the two nucleon interaction in order to evaluate its effects in the off-shell behavior of the t matrix. Secondly we investigate alternative numerical techniques to have a reliable evaluation of the off-shell properties and finally we analyze the differences we find in the off-shell behavior of various internucleon forces.

The first of the concerns, the two nucleon problem, has been studied extensively over the past 30 years both from a purely phenomenological viewpoint as well as with theories founded upon meson exchanges. More recently, new schemes which are hybrids of quantum chromodynamics (QCD) at short distances with one boson exchange potentials for the larger separations have been proposed. The Hamada-Johnston[6] and Reid[7] potentials are representative of the phenomenological viewpoint and are interactions still in use. Of the more modern NN interactions determined from field theoretic or dispersion relations techniques, the Bonn[8] and Paris[4] are widely quoted in literature, while the QCD based models[9] are as yet not so favored.

Whatever be the basis, all such NN interactions are determined from fits to the elastic NN phase shifts and the properties of the deuteron; such fits varying in quality between different interactions and for different two-body channels. The critical features of all interactions, whether contrived or derived, are the form factors. For this reason we consider herein the Reid interaction as being representative of the usual phenomenologically based interactions, the Paris as being representative of the derived interactions and a third which we have developed from a recent, momentum space, phenomenological model.[10] Our model interaction has a form factor with momentum transfer dependence additional to the usual one boson exchange potentials (OBEP) and is defined to obtain the best possible fits to all partial wave

two nucleon phase shifts up to 400 MeV laboratory energy as well as to fit the deuteron properties. Coincidentally, the phase shifts to 800 MeV are also well reproduced for most channels.

Specifically, our interaction uses three basic Yukawa factors $[q^2+m_i^2]^{-1}$ with ranges, m_i, that correspond to those of the one pion, two pion and ρ and ω mesons in meson exchange theory. Additionally, in each two nucleon channel these are modulated by a Gaussian dependence of the momentum transfer and one or more of a set of three simple scalar functions of momentum. Thereby we have an interaction that is markedly different to either the Reid or Paris interactions. Details are given in the next section (Sec. II).

All three interactions lead to (coupled) integral equations for their associated t matrices when developed in a momentum space representation and a standard method for the solution of such equations is that of matrix inversion.[11] We have used that method in this study, in addition, we have also used an alternate method involving continued fractions[12] but developed in a different, more facile way. Details of the two methods are specified in Sec. III. The two body data predictions (phase shifts to 800 MeV and deuteron properties) that result from the t-matrix calculations built upon each of the three chosen interactions are discussed in Sec. IV with the component attributes of our phenomenological interaction being interpreted as far as possible in terms of more commonly used operator expectation values.

Off shell characteristics of the t matrices are then discussed in Secs. V and VI; the former being restricted to the half-on-shell f ratios with which on-shell differences between the different t matrices are eliminated. The complete, off-shell and complex t matrices are displayed, compared, and their differences discussed, in Sec. VI.

II. EMPIRICAL NUCLEON-NUCLEON INTERACTION

Form factors have always been the crucial elements of two nucleon interactions. The (vertex) form factors, which account for the extended structure of the nucleon, are also required to regularize singularities of interactions derived from meson exchange theory.[8] As yet these form factors have not been specified by any underlying (QCD) formalism. One therefore has some liberty as to the choice of that form factor. Usually, they are chosen as the Yukawa form $[(\Lambda_n^2-m^2)/(\Lambda_n^2+\mathbf{q}^2)]^n$ where $n=\frac{1}{2}$, 1, $\frac{3}{2}$, and 2 though the Gaussian form, $\exp(-\mathbf{q}^2/\Lambda^2)$ is also suitable with Λ approximating to $\Lambda_n/\sqrt{n}$ from small $\mathbf{q}^2$ expansions.[22] The Gaussian form is also suggested when the connection between strong and electromagnetic interactions obtained by means of the eikonal approximation is used to constrain the parameters of nucleon-nucleon scattering.[23]

The notable feature of our interaction is its form factor; the choice of which in view of the foregoing was then predicated upon the known form of the forward scattering cross sections as functions of t $(=-\mathbf{q}^2)$. It is well known[16] that p-p scattering data, among others, exhibit the $\exp(Bt)$ behavior with B a different constant in each of three distinctive regimes. Then, as p-p scattering cross sections scale as the fourth power of the proton form factor, we have the basis for our choice of form factors in our empirical nucleon-nucleon interaction.

In a momentum space representation the force has the form

$$\hat{V}(\mathbf{k},\mathbf{k}')=\sum_{i=1}^{3}\hat{O}_i(\mathbf{k}',\mathbf{k})F_i(\mathbf{q}^2)\ , \tag{1}$$

where $\hat{O}_i$ are general momentum, spin and isospin dependent operators and $F_{(i)}$ is the "total" form factor which depends upon the transfer momentum $\mathbf{q}=\mathbf{k}-\mathbf{k}'$, as

$$F_i(\mathbf{q}^2)=\frac{1}{\pi^2}\frac{\hbar^2}{m}G\frac{M}{m_i}\exp\left[-\frac{M}{m_i}\right]\frac{\exp(-\mathbf{q}^2/2m_i^2)}{\mathbf{q}^2+m_i^2}\ . \tag{2}$$

In Eq. (2) m is twice the reduced nucleon mass $(m=M\hbar c)$, G is an overall constant (20.4 fm^{-1}) for all the states, and m_i define the basic scales and ranges of the interaction:

$$m_\pi=135.0/\hbar c\ \text{fm}^{-1},\quad m_\pi^{-1}=1.462\ \text{fm}\ ,$$
$$m_{2\pi}=279.1/\hbar c\ \text{fm}^{-1},\quad m_{2\pi}^{-1}=0.707\ \text{fm}\ ,$$
$$m_{\rho,\omega}=774.0/\hbar c\ \text{fm}^{-1},\quad m_{\rho,\omega}^{-1}=0.255\ \text{fm}\ ,$$
$$M=938.9/\hbar c\ \text{fm}^{-1},\quad \hbar c=197.33\ \text{MeV fm}\ .$$

In our approach, we take the eigenvalues of the operators $\hat{O}_i$ in Eq. (1) as free parameters which are determined by fitting the nucleon-nucleon phase shifts and the binding energy of the deuteron. As will be shown later, these eigenvalues are simple numbers as a result of the specific relative mass weighting used in Eq. (2).

The momentum dependence of the $\hat{O}_i$ operators required to fit the data is

$$\hat{O}_i(\mathbf{k}',\mathbf{k})=\hat{\alpha}_i+\hat{\beta}_i\frac{\mathbf{q}^2}{2m_i^2}+\hat{\gamma}_i\frac{\mathbf{k}\cdot\mathbf{k}'}{m_i^2}\ , \tag{3}$$

where $\hat{\alpha}_i$, $\hat{\beta}_i$, and $\hat{\gamma}_i$ are operators with eigenvalues to be determined.

The nucleon-nucleon interaction may be expanded in terms of the total angular momentum (J), the total orbital angular momentum (L), total spin (S), and total isospin (T) channels for the nucleon pair, namely,

$$\hat{V}(\mathbf{k}',\mathbf{k})=\frac{2}{\pi}\frac{\hbar^2}{m}\sum_{JN}\sum_{LL'ST}\mathcal{Y}^N_{JL'S}(\hat{\mathbf{k}}')V^{JST}_{L'L}(k,k')\times\mathcal{Y}^{N\dagger}_{JLS}(\hat{\mathbf{k}})\hat{P}_T\ , \tag{4}$$

with

$$\mathcal{Y}^N_{JLS}(\hat{\mathbf{k}})=\sum_{\mu\nu}\langle LS\mu\nu\,|\,JN\rangle Y_{L\mu}(\hat{\mathbf{k}})\,|\,S\nu\rangle\ , \tag{5}$$

and $\hat{P}_T$ is the total isospin projection operator. Therefore, from Eqs. (1) and (4) we have

$$V^{JST}_{L'L}(k',k)=\frac{\pi}{2}\frac{m}{\hbar^2}\sum_{i=1}^{3}\int d\hat{\mathbf{k}}'\int d\hat{\mathbf{k}}\,\mathcal{Y}^{N\dagger}_{JL'S}(\hat{\mathbf{k}}')\langle TT_3\,|\,\hat{O}_i(\mathbf{k}',\mathbf{k})F_i(\mathbf{q}^2)\,|\,TT_3\rangle\mathcal{Y}^{N}_{JLS}(\hat{\mathbf{k}})\ . \tag{6}$$

The explicit expressions for $V^{JST}_{L'L}$ are obtained by considering that

$$\frac{\exp(-\mathbf{q}^2/2m_i^2)}{\mathbf{q}^2+m_i^2}=\exp\left[-\frac{(k^2+k'^2)}{2m_i^2}\right]\frac{1}{2kk'}\times\sum_L(2L+1)P_L(\mu)I_L(x_i,z_i)\ , \tag{7}$$

with $P_L(\mu)$ being Legendre functions of the first kind, $\mu=\hat{\mathbf{k}}\cdot\hat{\mathbf{k}}'$, and I_L being the multipoles defined by

$$I_L(x,z)=\sum_{n,n'}(2n+1)\langle nL00\,|\,n'0\rangle^2 i_n(x)Q_{n'}(z)\ , \tag{8}$$

where the $\langle nL00\,|\,n'0\rangle$ are Clebsch-Gordan coefficients, the $i_n(x)$ are the modified spherical bessel functions of the first kind, and the $Q_n(z)$ are Legendre functions of the second kind.[13]

In Eq. (7) the variables x_i and z_i are (kk'/m_i^2) and $(k^2+k'^2+m_i^2)/(2kk')$, respectively. Furthermore it is simple to prove that

$$\frac{\hat{\mathbf{k}}\cdot\hat{\mathbf{k}}'\exp(-q^2/m_i^2)}{\mathbf{q}^2+m_i^2}=\exp\left[-\frac{(k^2+k'^2)}{2m_i^2}\right]\frac{1}{2kk'}\times\sum_L(2L+1)P_L(\mu)I'_L(x_i,z_i)\ , \tag{9}$$

where

$$I'_L(x,z)=\sum_{n,n'}(2n+1)\langle nL00\,|\,n'0\rangle^2\times i_n(x)[zQ_{n'}(z)-\delta_{n'0}]\ . \tag{10}$$

Collecting the results of Eqs. (2), (3), (7), and (9) we get for the diagonal interaction matrix elements [Eq. (4)]

$$V^{JST}_{LL}(k',k)=\sum_i\mathcal{G}_i(k,k')\left\{\alpha_i^{JLST}I_L(x_i,z_i)+\beta_i^{JLST}\left[\frac{(k^2+k'^2)}{2m_i^2}I_L(x_i,z_i)-\frac{kk'}{m_i^2}I'_L(x_i,z_i)\right]+\gamma_i^{JLST}\frac{kk'}{m_i^2}I'_L(x_i,z_i)\right\}, \tag{11}$$

with

$$\mathcal{G}_i(k',k)=\frac{1}{kk'}G\frac{M}{m_i}\exp\left[-\frac{M}{m_i}\right]\times\exp\left[-\frac{(k^2+k'^2)}{2m_i^2}\right]\ . \tag{12}$$

For the off-diagonal matrix elements $V^{JST}_{LL'}$, $L\neq L'$, which are due to tensor operators only, we replace the I_L function in Eq. (11) by I_J and consider only a q^2 dependence in the $\hat{O}_i$ operator. Therefore we have, for $L\neq L'$,

$$V^{JST}_{L'L}(k,k')=\sum_i\mathcal{G}_i(k,k')\beta_i^{JST}\left[\frac{(k^2+k'^2)}{2m_i^2}I_J(x_i,z_i)-\frac{kk'}{m_i^2}I'_J(x_i,z_i)\right]\ . \tag{13}$$

In Table I we have summarized the values obtained phenomenologically for the α, β, and γ coefficients in each state. By and large they are integer numbers and the fits shown later are those obtained when as many as possible have been constrained to have integer values. In view of the similarities to meson exchange potential effects we shall hereafter refer to the coefficients $(\alpha_i,\beta_i,\gamma_i)$ corresponding to the range parameter (m_i) as the "pion," "two pion," and "(ρ,ω)" contributions, respectively.

From Table I we observe that the "one pion" contribution only involves the $\hat{\alpha}_1$ operator $(\hat{\beta}_1=\hat{\gamma}_1=0)$ while the "two pion" and "(ρ,ω)" contributions are dominantly q^2 dependent $(\hat{\beta})$, with $(\hat{\alpha}_2=\hat{\alpha}_3=0)$ and with a few states requiring significant $\mathbf{k}\cdot\mathbf{k}'$ components in the "(ρ,ω)" contributions. The off-diagonal (tensor coupling) strengths are listed at the bottom of Table I.

III. THE FREE *t* MATRIX AND METHODS OF SOLUTION

The n-p scattering phase shifts are determined by the on-shell expectation values of the free two nucleon t matrix which in turn is derived from the expectation values of the complete T-matrix operator $\hat{T}(z)$ defined at energy z by

$$\hat{T}(z)=\hat{V}+\hat{V}\lim_{\eta\to0}(z-\hat{K}_1-\hat{K}_2+i\eta)^{-1}\hat{T}(z)\ , \tag{14}$$

in which $\hat{V}$ is the (momentum space) two nucleon interaction and $\hat{K}_i$ is the kinetic energy operator for a free particle of mass m_i. Hereafter the limit will be taken as assumed whenever appropriate.

Transformed to relative and center of mass variables, $(\mathbf{k}_1-\mathbf{k}_2)/2$ and $(\mathbf{k}_1+\mathbf{k}_2)$, respectively, for equal mass particles, we get

$$\langle\mathbf{k}'_1\mathbf{k}'_2\,|\,\hat{V}\,|\,\mathbf{k}_1\mathbf{k}_2\rangle=\langle\mathbf{k}'\,|\,\hat{V}\,|\,\mathbf{k}\rangle\delta(\mathbf{K}'-\mathbf{K})\ , \tag{15}$$

and with

$$\langle\mathbf{k}'\mathbf{K}'\,|\,\hat{T}(z)\,|\,\mathbf{k}\mathbf{K}\rangle=\delta(\mathbf{K}'-\mathbf{K})\langle\mathbf{k}'\,|\,t(\omega)\,|\,\mathbf{k}\rangle\ , \tag{16}$$

wherein with μ being the reduced mass $(m/2)$, and M, the total mass of the scattering pair

TABLE I. Interaction strength coefficients.

State	α_1	β_1	β_2	γ_2	β_3	γ_3
$^1S_0$	−4		−1	0.3	5.4	5.4
$^1D_2$	−0.7		0.8	0	16	4
$^1G_4$	−0.7		0.6	0	25	5
$^1I_6$	−0.7		0.5	0	42	5
$^1P_1$	2		1.4	0.4	−6	0
$^1F_3$	2		−0.6	0	−30	−10
$^1H_5$	2		0	0	−90	0
$^1K_7$	2		0	0	−168	0
$^3S_1$	−6		−2	0.5	4	−1
$^3D_1$	4		−3	0.1	−34	0
$^3D_2$	−2		5.5	0	30	5
$^3D_3$	0.4		1.2	0	10	3
$^3G_3$	1		−2.5	0	−30	0
$^3G_4$	−2		5	0	20	1
$^3G_5$	0		−0.5	0	3	0
$^3I_5$	1		−1.8	0	−20	0
$^3I_6$	−2		6	0	15	0
$^3P_0$	−1.7		2	0	30	30
$^3P_1$	0.7		−1.5	0	−8	8
$^3P_2$	0		0.5	0	7.4	0
$^3F_2$	0		1.4	0	−8	0
$^3F_3$	0.7		−1.8	0	20	10
$^3F_4$	0		0.8	0	18	4
$^3H_4$	0		1.2	0	−10	0
$^3H_5$	0.7		−2	0	20	0
$^3H_6$	0		0.7	0	15	0
$^3K_6$	0		1	0	−8	0
$^3K_7$	0.7		−2	0	15	0
ϵ_1		2	0		4	
ϵ_2		−1.5	−1.6		−4	
ϵ_3		5.6	4		22	
ϵ_4		−2	−1.3		−7	
ϵ_5		6	3.6		25	
ϵ_6		−2	−2		−10	

$$\omega = z - (\hbar^2 K^2/2M) , \tag{17}$$

so that $\hat{t}(\omega)$ satisfies the integral equation

$$\langle \mathbf{k}' | \hat{t}(\omega) | \mathbf{k} \rangle = \langle \mathbf{k}' | \hat{V} | \mathbf{k} \rangle + \int d\mathbf{q} \langle \mathbf{k}' | \hat{V} | \mathbf{q} \rangle [\omega - (\hbar^2 q^2/2\mu) + i\eta]^{-1} \langle \mathbf{q} | \hat{t}(\omega) | \mathbf{k} \rangle . \tag{18}$$

The elastic scattering amplitude then relates to the on shell ($|\mathbf{k}'| = |\mathbf{k}|$; $\omega = \hbar^2 k^2/2\mu = E_{\text{lab}}/2$) antisymmetrized matrix elements of $\hat{t}(\omega)$ by

$$f(\mathbf{k}',\mathbf{k}) = -\frac{4\pi^2\mu}{\hbar^2} \langle \mathbf{k}' | \hat{t}(\omega) | \mathbf{k} \rangle_A . \tag{19}$$

Solutions of the t-matrix equation are facilitated by using partial wave expansions

$$\langle \mathbf{k}' | \hat{X} | \mathbf{k} \rangle = \frac{1}{\pi} \frac{\hbar^2}{\mu} \sum_{\substack{JST \\ LL'N}} \mathcal{Y}^N_{L'SJ}(\hat{\mathbf{k}}') X^{JST}_{L'L}(k',k;\omega) \times \mathcal{Y}^{N\dagger}_{LSJ}(\hat{\mathbf{k}}) \hat{P}_T , \tag{20}$$

in which $\hat{P}_T$ are the two body isospin (T) projection operators, and L' and L are two particle orbital angular momentum quantum numbers, each of which combine with the two body spin (S) to give the angular momentum (J) of the two body system. Consequently we seek solutions of the (coupled) two body channels equations

$$t^{JST}_{L'L}(k',k;\omega) = V^{JST}_{L'L}(k',k) + \frac{2}{\pi} \sum_l \int V^{JST}_{L'l}(k',q)[q_0^2 - q^2 + i\eta]^{-1} \times t^{JST}_{lL}(q,k;\omega) q^2 dq , \tag{21}$$

in which

$$\omega=\hbar^2 q_0^2/2\mu \ . \tag{22}$$

Two quite distinctive methods of solution have been used to determine the results we present herein. The first method is that of matrix inversion as used previously, for example, by Haftel and Tabakin[11] in their studies of the two nucleon problem. A brief review of this method is given in the next section. The second method is that of continued fractions; a detailed discussion of which (with respect to solutions of the above, specific, integral equations) is also given in the next section of this paper.

By using two methods of solution and comparing t matrices that result not only can we gauge the accuracy of the first used (matrix inversion) calculations but also can we be confident that the solutions have converged. Furthermore, mindful of the repetitive use of these calculations to provide the elemental t matrices required in analyses of the many body problem (e.g., specification of the nuclear optical potential) it is worthwhile to investigate the relative computation times of the different methods.

A. Matrix inversion method

The standard method used herein follows the procedure that was used by Haftel and Tabakin.[11] Instead of solving directly for the complex t-matrix elements, an intermediate purely real reaction matrix corresponding to standing wave boundary conditions is defined. Following the same steps leading to Eq. (21) yields

$$R^{JST}_{L'L}(k',k;\omega)= V^{JST}_{L'L}(k',k) + \frac{2}{\pi}\sum_l \mathrm{P}\int V^{JST}_{L'l}(k',q)[q_0^2-q^2]^{-1} \times R^{JST}_{lL}(q,k;\omega)q^2dq \ , \tag{23}$$

where P is the principal value operator.

By defining a suitable grid of $(N-1)$ integration points (Gauss-Legendre or Gauss-Laguerre) in momentum space to span the interval contributing to the integral, subtracting a suitable pole term, and solving Eq. (23) for a column vector or matrix of $R^{JST}_{L'L}(k',k;\omega)$ values, the problem is reduced to an inversion of an $N\times N$ matrix for uncoupled channels and a $2N\times 2N$ matrix for coupled channels.

From the identity

$$\lim_{\eta\to 0}\int dx\, f(x)(x-x_0+i\eta)^{-1} = \mathrm{P}\int f(x)(x-x_0)^{-1}dx - i\pi f(x_0) \ , \tag{24}$$

the complex elements of the t matrix corresponding to outgoing boundary conditions can be shown to be,

$$t^{JST}_{L'L}(k',k;\omega)=R^{JST}_{L'L}(k',k;\omega) - iq_0\sum_l R^{JST}_{L'l}(k',q_0;\omega) \times t^{JST}_{lL}(q_0,k;\omega) \ . \tag{25}$$

Thus the half-on-shell solutions of Eq. (25) which are found by simple inversion can be substituted back to specify the complete off-shell behavior of the t matrices.

In their recent study of the two nucleon $K(R)$ matrix, Redish and Stricker-Bauer[17] obtained solutions to Eq. (23) to accuracies of 1:1000 or better. They used different integration techniques from which they assessed that the Haftel-Tabakin procedure may give problems in maintaining accuracy. Any such problem we observe is primarily due to the choice of matrix inversion algorithm. Our results converged quickly with Gauss-Laguerre quadratures of 24 to 32 points when the International Mathematical and Statistical Libraries, Inc. (IMSL) library matrix routine that features iterative refinement was used.

B. Method of continued fractions

The method of continued fractions (MCF) has been used by Horáček and Sasakawa[12] to study problems in atomic physics and, more recently, to investigate t matrices from local and nonlocal potentials in the two nucleon problem. However, this formalism is rather cumbersome and so we propose an alternative scheme for use of this method to specify t matrices. Furthermore a recent comparison[18] of the continued fractions, Padé approximant, and iterative-subtractive[19] methods of solution starting with the Reid soft core interaction demonstrated that all such methods converged, albeit that the continued fractions methods of Horáček and Sasakawa did so slowly. The use of a successive substitution process[12] was deemed to be the cause of that slow convergence. We do not use that process.

Consider a formal solution of the t matrix equation (14) which has the form

$$\hat{t}(\omega)=[1-\hat{W}(\omega)]^{-1}\hat{V} \ , \tag{26}$$

wherein, with $\hat{G}$ being the free particles' Green's function,

$$\hat{W}(\omega)=\hat{V}\,\hat{G}(\omega) \ . \tag{27}$$

In partial wave expansion we then get the solutions of

$$t^{JST}_{L'L}(k',k;\omega)=\frac{\mu\pi}{\hbar^2}\int d\hat{\mathbf{k}}'\int d\hat{\mathbf{k}}\,\mathcal{Y}^{M\dagger}_{L'SJ}(\hat{\mathbf{k}}')\langle TT_z \mid \langle \mathbf{k}' \mid [1-\hat{W}(\omega)]^{-1}\hat{V} \mid \mathbf{k}\rangle \mid TT_z\rangle \mathcal{Y}^{M}_{LSJ}(\hat{\mathbf{k}})$$

$$\equiv[\tilde{N}^{\dagger}_0(k';JL'ST)N_0(k;JLST)]^{-1}\langle \tilde{D}_0(k';JL'ST) \mid [1-\hat{W}(\omega)]^{-1} \mid D_0(k;JLST)\rangle \ , \tag{28}$$

in which $|\tilde{D}_0\rangle, |D_0\rangle$ are members of a biorthogonal basis for each set of quantum numbers (JST) and which satisfy

$$\sum_j |D_j\rangle\langle\tilde{D}_j| = 1 , \tag{29}$$

$$\langle\tilde{D}_i | D_j\rangle = \delta_{ij} , \tag{30}$$

when other elements are defined by

$$|D_i(k,L)\rangle = N_i(k,L)\left[\hat{W}(\omega)|D_{i-1}(k;L)\rangle - \sum_{j=0}^{i-1}|D_j(k;L)\rangle W_{ji-1}\right] , \tag{31}$$

and

$$|\tilde{D}_i(k',L')\rangle = \tilde{N}_i(k',L')\left[\hat{W}^\dagger(\omega)|\tilde{D}_{i-1}(k';L')\rangle - \sum_{j=0}^{i-1}|\tilde{D}_j(k';L')\rangle W^\dagger_{i-1j}\right] . \tag{32}$$

The elements, W_{ij}, form a tridiagonal matrix since

$$W_{ij} = \langle\tilde{D}_i(k';L')|\hat{W}(\omega)|D_j(k;L)\rangle = 0 \text{ if } |i-j|>1 , \tag{33}$$

and, as a consequence, we obtain the continued fraction specification of the t matrices (for each JST combination), viz.,

$$t_{L'L}(k',k;\omega) = [\tilde{N}^\dagger_0(k';L')N_0(k;L)]/f_\infty , \tag{34}$$

where

$$f_\infty = b_0 - \{a_1/[b_1 - a_2/(b_2 - \cdots)]\} , \tag{35}$$

and

$$b_i = 1 - W_{ii}(k',k;L'L) , \tag{36}$$

$$a_i = W_{i-1i}(k',k;L'L)W_{ii-1}(k',k;L'L) . \tag{37}$$

In principle, one would make an explicit construction of the basis, determining the normalization coefficients, and thus evaluate matrix elements of $\hat{W}(\omega)$. But there is an alternative and more practical procedure to determine the tridiagonal matrices and thus the continued fractions to specify the t matrices. This procedure is independent of the explicit state normalizations.

Consider the state vectors

$$|d_0(k;LJST)\rangle = |D_0(k;JLST)\rangle/N_0(k;JLST) \equiv \frac{\pi\mu}{\hbar^2}\int d\hat{\mathbf{k}}\,\hat{V}|\mathbf{k}\rangle|TT_z\rangle\mathcal{Y}^M_{LSJ}(\hat{\mathbf{k}}) , \tag{38}$$

and

$$|\tilde{d}_0(k',JL'ST)\rangle = |\tilde{D}_0(k';JL'ST)\rangle/\tilde{N}_0(k';JL'ST) \equiv \int d\hat{\mathbf{k}}'|\mathbf{k}'\rangle|TT_z\rangle\mathcal{Y}^M_{L'SJ}(\hat{\mathbf{k}}') , \tag{39}$$

in terms of which the diagonal matrix elements, W_{pp}, can be expressed as

$$W_{pp} = \langle\tilde{d}_0(k';L')|\hat{F}_p\hat{W}\hat{F}_p|d_0(k;L)\rangle/\langle\tilde{d}_0(k';L')|\hat{F}_p\hat{F}_p|d_0(k;L)\rangle , \tag{40}$$

and the required product of off-diagonal elements becomes

$$W_{p-1p}W_{pp-1} = \langle\tilde{d}_0(k';L')|\hat{F}_p\hat{F}_p|d_0(k;L)\rangle/\langle\tilde{d}_0(k';L')|\hat{F}_{p-1}\hat{F}_{p-1}|d_0(k;L)\rangle , \tag{41}$$

with operators defined by

$$\hat{F}_p = \sum_{n=1}^{p+1}\alpha_n(p)(\hat{W})^{p+1-n} \tag{42}$$

involving coefficients that are obtained by a recursion

$$\alpha_n(p) = \alpha_n(p-1) - (W_{p-1p-1})\alpha_{n-1}(p-1) - (W_{p-2p-1}W_{p-1p-2})\alpha_{n-1}(p-2) , \tag{43}$$

with starting values

$$\alpha_1(p) = \alpha_1(p-1) = 1, \quad \alpha_{p-2}(p) \equiv 0 . \tag{44}$$

The t matrices expressed as per Eq. (28) are thus independent of all normalization products, $[\tilde{N}^\dagger_i(k';L')N_i(k;L)]$, and the entries in the continued fraction require evaluation of matrix elements of the form ($N = 1,2,\ldots$)

$$I^{(N)}_{L'L}(k',k) = \langle\tilde{d}_0(k';L')|(\hat{W})^N|d_0(k;L)\rangle . \tag{45}$$

The continued fraction is easily summed via a recursion formula[13] for its mth convergent. Given that the limit $m\to\infty$ exists, convergence to that value is very rapid in the calculations we have made. This procedure has the added advantage that one need only evaluate an additional set of basic elements, $I^{(N)}_{L'L}$ to incorporate the next term in the continued fraction sum since (for each JST)

$$I^{(N)}_{L'L}(k';k) \equiv \frac{2}{\pi}\sum_l\int V_{L'l}(k',q)[q_0^2 - q^2]^{-1}I^{(N-1)}_{lL}(q;k)q^2dq , \tag{46}$$

with

$$I^{(0)}_{L'L}(k',k) \equiv V_{L'L}(k',k) , \tag{47}$$

and

$$\langle\tilde{d}_0(k';L')|\hat{F}_p\hat{W}\hat{F}_p|d_0(k;L)\rangle = \sum_{n,n'=1}^{p+1}\alpha_{n'}(p)\alpha_n(p)I^{(N)}_{L'L}(k',k) , \tag{48}$$

with

$$N = 2p + 3 - n - n' \ . \tag{49}$$

IV. THE ON-SHELL t MATRIX

A. Phase shifts and deuteron properties

The nuclear bar phase shifts as determined by the single energy analysis of Arndt *et al.*[14] of elastic n-p scattering are shown as the error bar data in Figs. 1 and 2 for each two body channel or coupling parameter as designated in each panel. These phase shifts are compared with the results obtained using the Reid, Paris and our interactions and identified by the dot-dash, broken, and continuous curves, respectively. The results are displayed up to a laboratory energy of 800 MeV to stress some of the strong effects of the "(ρ,ω)" contributions even though, in some channels, the imaginary parts of the phase shifts become significant for energies in excess of 400 MeV. Thus, to determine the parameters of our interaction the phase shift values to 400 MeV were used. It transpired that for most channels a good fit was then obtained up to 800 MeV. Adjustments were then allowed to ascertain the final parametrization with which the fits to phase shifts as displayed in the diagrams were obtained. By and large those adjustments were minor and to the "(ρ,ω)" contributions.

In each of the figures the very recent data of Arndt *et al.*[14] are displayed by the open circles or triangles whenever there is significant variation upon the earlier published values. Error bars have not been shown for

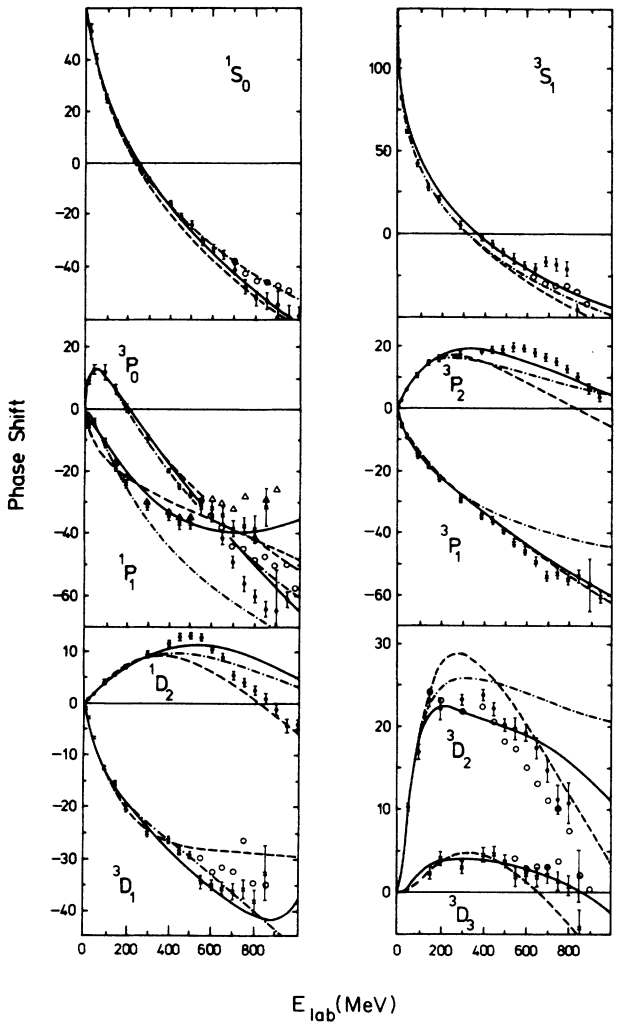

FIG. 1. The phase shifts from each two nucleon scattering state (as specified) and the predictions of them found using the Reid, Paris, and our interactions. These results are designated by the dot-dash, broken, and continuous curves, respectively. The more recent phase shift values of Arndt *et al.* (Ref. 14) are shown, without error bars, by the open circles or triangles.

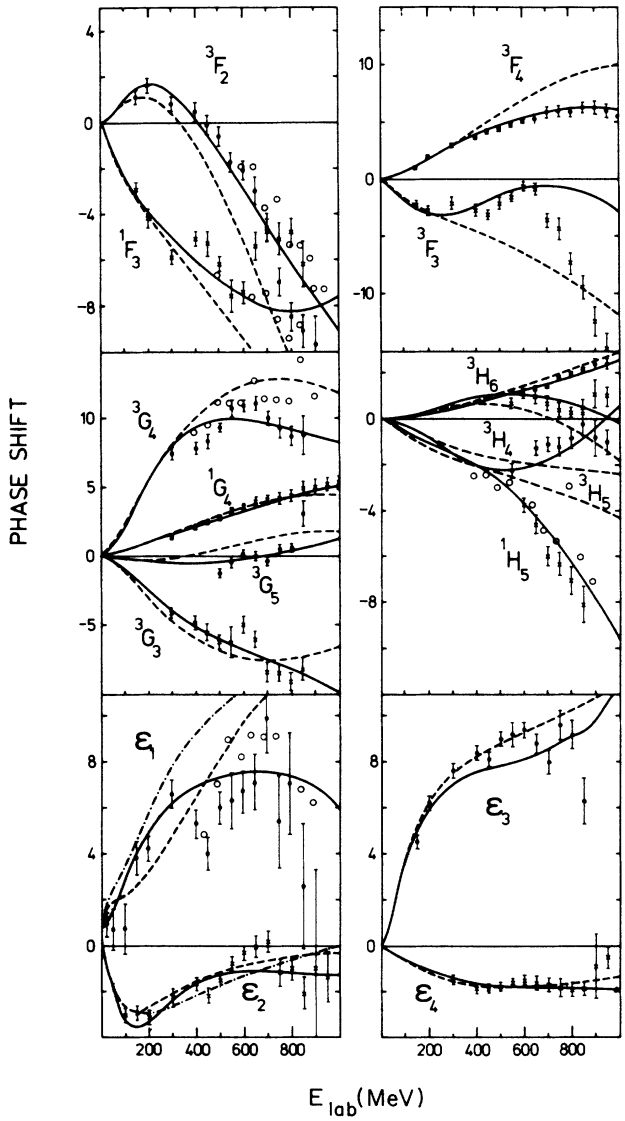

FIG. 2. The phase shifts from higher partial waves and the energy variations of the coupling parameters (ϵ) compared with the predictions obtained using the Reid, Paris, and our interactions as designated in Fig. 1.

these recent data. Neither were they used in our determination of the interaction.

Figure 1 displays the two nucleon S-, P-, and D-state results. It is quite evident that the three interactions give very similar and good fits to the data for the $^1S_0$, $^3S_1$, $^3P_0$, and $^3P_1$ channels. The most noticeable disagreements are in the results for the $^1P_1$ channel and at all energies. The D-state comparisons are quite reasonable save for the $^3D_2$ channel.

The coupling parameters and F, G, and H phase shifts are displayed in Fig. 2. In all cases and for all energies our interaction gives results in best agreement with the data of Arndt *et al.*

In view of the coupling in the $^3S_1$-$^3D_1$ channel, overall comparisons of the $^3S_1$,$^3D_1$ phase shifts and of the ϵ_1 coupling parameter are very important tests of an interaction. Our force, by such a test, is quite clearly a very good one which it should be since it is defined to give good fits to such data.

To add to the credibility of our interaction, we stress that, with its simple form and with the constraints that phase shift data to 400 MeV be well reproduced, it gives good low energy n-p predictions. Those results are displayed in Table II for the scattering lengths, effective ranges, and the deuteron binding energy. There is obviously a good comparison with the empirical values when the interaction strengths are primarily determined by fits to the $^3S_1$, $^3D_1$, and ϵ_1 energy variations.

Our deuteron S-state wave function is very similar to that obtained from either the Reid or the Paris potential but our D-state wave function is very small, giving a D-state probability of but 0.1%. Neither the use of enhanced ϵ_1 interaction channel strengths nor the addition of tensor functional forms (as in the Reid or Paris interactions) to our interaction in lieu of the multipoles $I_J(x_i,z_i)$ of Eq. (13) gave any significant increase in this D-state probability. As a consequence our interaction gives a ratio (A_D/A_S) of about one-half of the experimental value, and even though the value of ϵ_1 (0.2°) at 1 MeV appears to be in accord with the quadrupole moment,[15] our calculated value (of Q_D) is only 20% of the empirical number.

Notwithstanding that our interaction has been developed in a channel by channel basis and so could be nonlocal in the extreme, the resulting force is remarkably simple. With but three ranges, the component scaling and the form factor we have chosen has led to fitting coefficients (α,β,γ) that do not vary widely and are characteristic of simple operator expectation values.

TABLE II. Low energy results and deuteron properties.

Quantity	Expt.	Theory
α_s (np) (fm)	-23.7 ± 0.1	-24.7
α_t (fm)	5.42 ± 0.03	5.50
r_s	2.8	3.4
r_t	1.75	1.72
E_D (MeV)	2.2246	2.222

B. Component contributions

As with the OPEP the "one pion" components of our interaction are the dominating terms in the calculations of the low energy phase shifts (<50 MeV). The interaction strengths ($L>0$) in singlet states scale as expectation values of an operator of the form $\tau_1\cdot\tau_2$ and, in our interaction, their absolute strengths are very similar to the central part of the OPEP. Our S-state strengths (for both the $^1S_0$ and $^3S_1$ channels) are larger than the corresponding OPEP values, as is necessary to fit the low energy phase shift data. For the other triplet states the "one pion" strengths of our interaction appear to scale as a quadratic spin-orbit force.[10]

The "two pion" components of our interaction are very significant in the fits to phase shifts above 50 MeV. For most of the triplet states, it dominates fits to the data in the region between 100 and 200 MeV. Therein a consequence of the multipole identity, Eq. (10), becomes evident with the (positive) q^2 dependence being repulsive in effect for S states but attractive at low energies for other partial waves. With increasing energy these contributions become repulsive changing sign in the vicinity of 150, 350, and 600 MeV for the P, D, and F states, respectively. As with the "one pion" component there is no apparent need for diagonal tensor contributions as the triplet interaction strengths scale quite well with the expectations of $\tau_1\cdot\tau_2$ and quadratic spin-orbit operators.

The "(ρ,ω)" contributions in our interaction are very important for the S states, but for all higher partial wave states become important only above 200 MeV, dominating phase shift evaluations by and above 400 MeV. The component interaction strengths may no longer scale in accordance with the expectation values of simple scalar operators. And in any event, above 400 MeV the problem of absorption will have to be addressed before any of the data may be used to delineate interactions.

V. THE HALF-ON-SHELL t MATRIX

Before presentation and discussion of the off-shell variation of the t matrix, it is useful to seek a measure by which the fully-on-shell variations between the three interactions are eliminated from consideration, and from which off-shell trends may then be estimated. Such a measure is provided by the half-on-shell f ratio defined by

$$f^{JST}_{L'L}(k,q_0;\omega)=t^{JST}_{L'L}(k,q_0;\omega)/t^{JST}_{L'L}(q_0,q_0;\omega)\ , \qquad (50)$$

and which it is appropriate to specify as Kowalski-Noyes functions.[20] For an uncoupled channel, it is easy to show that these Kowalski-Noyes functions are purely real. Furthermore they relate, via unitarity to the imaginary part of the complete off-shell t matrix itself. This relationship and its consequence will be described in the next section of this paper.

For the coupled channels, however, these quantities remain complex and are not suitable for the simple assessments we seek at this stage. In those cases, it is convenient to consider instead the ratio of R-matrix elements,

$$f^{JST}_{L'L}(k,q_0;\omega)=R^{JST}_{L'L}(k,q_0;\omega)/R^{JST}_{L'L}(q_0,q_0;\omega)\ , \quad (51)$$

as did others[21] who studied these quantities. Thus we retain the terminology of "f ratios" to identify the appropriate real functions for any channel.

The f ratios are displayed in Figs. 3—6; the first two depicting the values for the uncoupled channels $^1S_0$ and $^1P_1$ and $^3P_{0,1}$, respectively, whilst the $^3S_1$ and $^3D_1$ results are shown in Fig. 5 and the off-diagonal cases are given in Fig. 6. In each figure the top, middle, and bottom sets of diagrams are the results for k ranging from 0 to 10 fm^{-1} and with on-shell values of q_0 of 0.11, 1.1, and 2.2 fm^{-1} coinciding with center of mass energies, ω, of 0.5, 50.0, and 200.0 MeV, respectively. Once again, the continuous, broken, and dot-dashed lines represent the f ratios found by using our, the Paris, and the Reid interactions, respectively.

The $^1S_0$ and $^1P_1$ half-on-shell f ratios are given in Fig. 3. For the $^1S_0$ case all interactions give quite similar results in the 0.5 and 50 MeV calculations and display some variation at the highest (200 MeV) energy. Around the on-shell values the Reid and Paris results are very similar at all energies, while our interaction (in that region) has a sharper variation at 0.5 MeV, a smoother variation at 50 MeV, and a mixed result at 200 MeV by comparison. In the high momentum region for all energies, our interaction gives a more gradually decreasing $^1S_0$ f ratio than either of the Reid or Paris re-

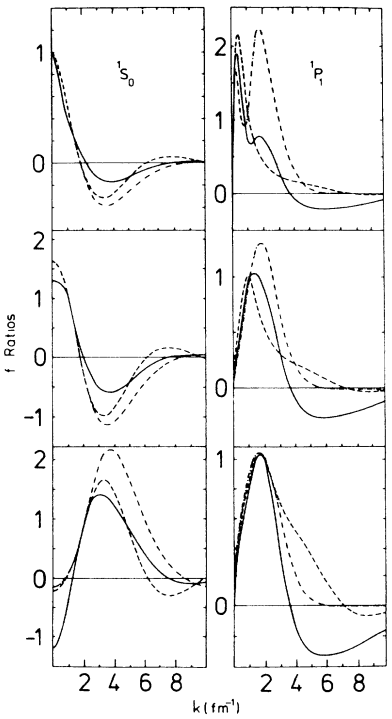

FIG. 3. The f ratios for the $^1S_0$ and $^1P_1$ states obtained from the t-matrix calculations with center of mass energies 0.5 ($q_0=0.11$, top), 50.0 ($q_0=1.1$, middle), and 200.0 ($q_0=2.2$, bottom) MeV.

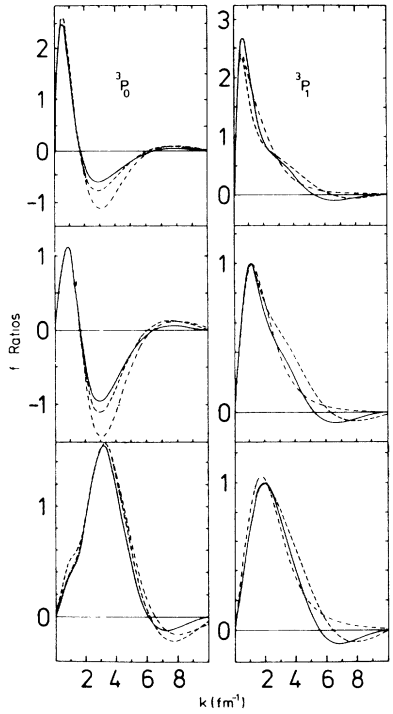

FIG. 4. The f ratios for the $^3P_0$ and $^3P_1$ states.

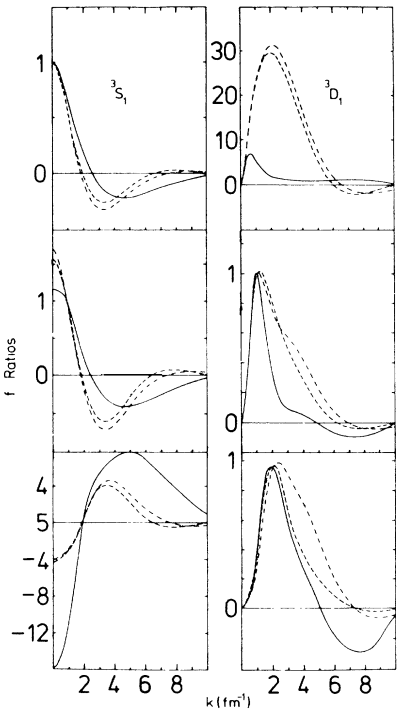

FIG. 5. The f ratios for the $^3S_1$ and $^3D_1$ (diagonal) states.

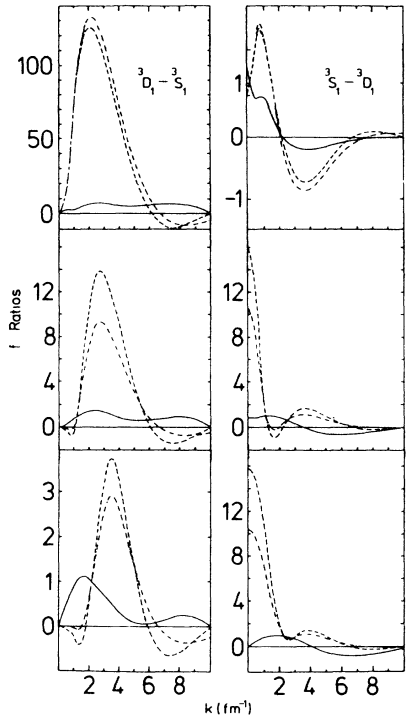

FIG. 6. The f ratios for the off-diagonal elements relating to the coupling parameter ϵ_1.

sults. In this channel, it is to be remembered, all three interactions give very good fits to the phase shift data. Such is not the case for the $^1P_1$ channel, particularly at low energies, and that disparity is reflected in the relevant f ratios shown in Fig. 3. At 0.5 and 50 MeV the f ratio of our (phase shift fit) interaction differs from both the Reid and Paris f ratios (which are distinctly different to each other as well). At low energy and momenta the Paris f ratio is an approximation to ours—but the Reid interaction gives better phase shift predictions than the Paris interaction at low energies. The reverse is true at the highest energy (200 MeV). We note that our interaction $^1P_1$ f ratio at all energies has a zero value at k of 4 fm^{-1}; a feature that is distinctively different from either the Reid or Paris results, and one which has a consequence in the full-off-shell t matrix.

The $^3P_0$ and $^3P_1$ f ratios are shown in Fig. 4. Therein the energy sequence and curve identification is as used in the discussion of Fig. 3. For both of these states, all interactions give excellent fits to the phase shift data over the 0 to 400 MeV (lab) energy range as is evident from Fig. 1, and in these cases the f ratios for all interactions are also very similar. The $^3P_0$ ratios, like $^1S_0$ ratios given in Fig. 3 and like the $^3S_1$ ratios to be discussed next, have a "repulsive" low momentum (<2 fm^{-1}) and an "attractive" higher momentum ratio at 0.5 and 50 MeV. For the 200 MeV case, however, the "repulsion" has spread to 6 fm^{-1} or even reversed roles with the "attractive" part. Major variation in the complete off-shell t matrices with energy may be anticipated in these channels. That is not likely to be the case for the $^3P_1$ state given the structural similarity of the f ratios and at all energies. Other channels such as the $^3D_2$ show behavior like the $^3P_1$ state variation and will not be shown.

The $^3S_1$ and $^3D_1$ state f ratios are shown in Fig. 5 and it is clear that at all energies the Reid and Paris results are very similar. That is also the case for the off-diagonal f ratios shown in Fig. 6. It is also clear that our interaction, by comparison, has quite different variations. The $^3S_1$ f ratios of our interaction are not as sharply varying with momenta as the others at 0.5 and 50 MeV, but there is complete change in the 200 MeV results. However, at this energy our phase shift value is very small and the associated on-shell R-matrix element is thus very small as well. At the low energies our interaction f ratios cross the axis at around 2.8 fm^{-1}, but for the 200 MeV case this crossover occurs much closer to the 2.0 fm^{-1} value at which the Paris and Reid f ratios have their zeroes. But the major difference occurs in the $^3D_1$ (and off-diagonal cases) at 0.5 MeV. The Paris (Reid) $^3D_1$ f ratios vary by a factor of 30 away from the on-shell point. Our result is far less severe. At the higher energies, the Paris and Reid variations are no longer so severe but yet are quite different to our result which changes sign at 5 fm^{-1}. The off-diagonal results show even more pronounced size variation in the f ratios determined from the Reid and Paris interactions whereas our force is far smoother. Large scale variations in the complete off-shell t matrices will not be unexpected therefore.

Clearly then data that is sensitive to the off-shell behavior (of a tensor force) will distinguish between our interaction and either the Reid or Paris interaction t matrices. Indeed very large differences would result if such data stressed the low energy off-diagonal channel character.

VI. OFF-SHELL CHARACTER OF THE t MATRIX

The off-shell properties of the two nucleon t matrix, $t^{JST}_{L'L}(k',k)$ as defined by Eq. (21), have been calculated for the Paris, Reid, and our interaction forms at center of mass energies, ω, of -50 MeV (for which one obtains the, purely real, G matrix), and 0.5, 50, and 200 MeV. The real and imaginary parts of those t matrices have been separated and their variations found in graphical forms for the range of momenta (k,k') from 0 to 9 fm^{-1}. The results are depicted in Figs. 7—18, in which, except when specified to the contrary, the t-matrix elements as shown by our interaction are given in the left-hand panel from top to bottom in increasing energy (ω). The right (of two) or center (of three) panels in the diagrams give the results we obtained by using the Paris interaction while the right (of three) panels give the results found starting with the Reid interaction.

In making these plots, different scales have been chosen to ensure that the t-matrix structure can easily be observed. The same scale is used for all energies in any channel, however. But the imaginary parts of the t matrices have quite different energy variation between channels, whence plots will be given of $q_0^n \mathrm{Im}(t)$ with n being $0, \pm 1$ as is relevant. All scales for the channels to

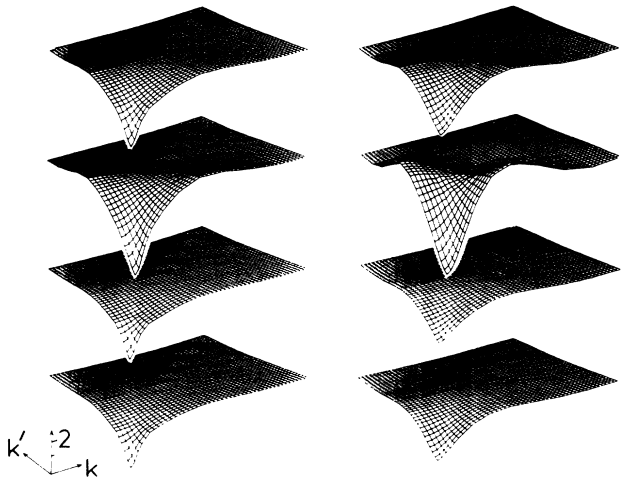

FIG. 7. The real parts of the Paris (right panel) and our (left panel) interaction t matrices in the $^1S_0$ channel. From top to bottom are shown the results found using a center of mass energy (ω) of -50.0, 0.5, 50.0, and 200.0 MeV.

be presented are given in Table III. Clearly the S channels dominate by as much as an order of magnitude in the energy regime (to 200 MeV in the center of mass.)

Unitarity leads to the interesting result for the imaginary parts of the off-shell t matrix, namely

$$\mathrm{Im}[t^{JST}_{L'L}(k',k;\omega)] = -q_0 \sum_l t^{JST*}_{L'l}(k',q_0;\omega) t^{JST}_{lL}(q_0,k;\omega) \ . \tag{52}$$

Thus, for uncoupled states at least, if the real part of the t matrix is zero at some half-on-shell value of k [$t^{JST}_{L'L}(q_0,k;\omega)=0$] then for all k' at that value of k we will get a nodal line in the imaginary part of that t matrix. Further, in such cases the imaginary part of the t matrix is separable. Such symmetry provides a check upon our evaluations of the t matrices the results of which are now discussed.

The off-shell variation of the t-matrix elements for the $^1S_0$ channel are displayed in Fig. 7 (the real part) and

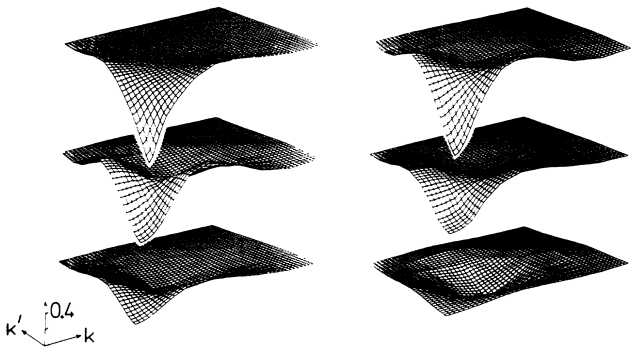

FIG. 8. The $n=1$ type imaginary parts of the $^1S_0$ t matrices relevant to the positive energy parts of Fig. 7.

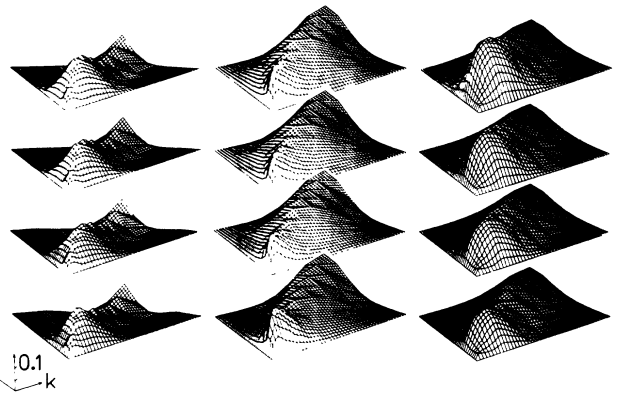

FIG. 9. The real parts of the Reid (right panel), Paris (center panel), and our interaction (left panel) t matrices in the $^1P_1$ channel for the sequence of center of mass energies used in Fig. 7.

Fig. 8 (the imaginary part of $n=1$ type.) As with the $^3S_1$ channel matrix elements, these matrix elements have on-shell values that are significant in two nucleon scattering at all energies as is evident by the phase shifts shown in Fig. 1. On the other hand, the half-on-shell f ratios (Fig. 3) revealed differences between our interaction and those of Reid or the Paris group; both of which interactions gave very similar f ratios. It is no surprise therefore to find that the full-off-shell variations of the Paris and Reid $^1S_0$ t matrices are also very similar; so similar in fact that the Reid results are not displayed in Figs. 7 and 8. But the Paris and our interactions have quite different form and so the similarity of the off-shell behavior of their t matrices as shown in figures may not have been expected.

The real part of the $^1S_0$ t matrices have a deep attraction at small momenta (<2 fm^{-1}) which is weakly dependent upon the center of mass energy ω. The imaginary parts of the $^1S_0$ t matrices are more obviously energy dependent with the most marked change occurring in the Paris results for ω between 50 and 200 MeV. Nevertheless a similar variation occurs in the t matrices obtained with our interaction reflecting the change in sign of the (on-shell) $^1S_0$ phase shifts at $\omega \sim 125$ MeV.

The relationships between the nodal lines in the imaginary t matrix and the half-on-shell, real part of the t ma-

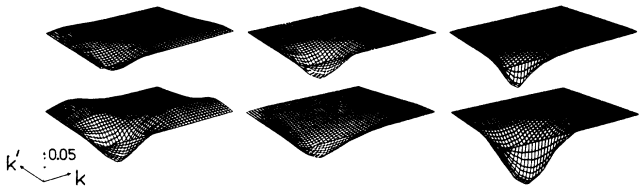

FIG. 10. The imaginary (type $n=-1$) $^1P_1$ channel t matrices from our, Paris and Reid interactions (left to right) and at energies of 50 and 200 MeV (top to bottom).

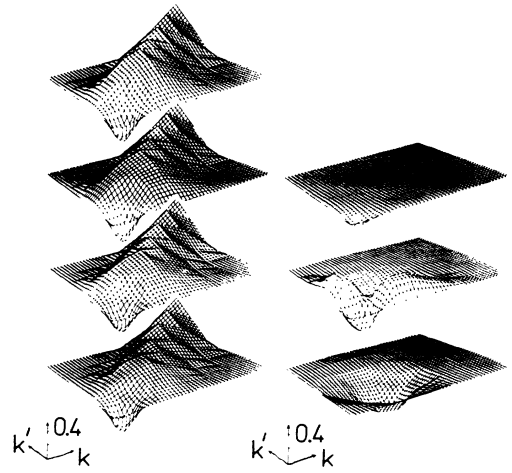

FIG. 11. The $^3P_0$ t matrices obtained using our interaction. The real parts are for energies -50, 0.5, 50, and 200 MeV are shown from top to bottom in the left-hand panel. The imaginary (type $n=-1$) parts for the positive energy sequence are shown on the right.

trix as a consequence of unitarity are evident in these figures but are more visible in other channel results.

The t matrices for the $^1P_1$ channel are displayed in Fig. 9 (real) and Fig. 10 (imaginary for $n=-1$). The magnitude variations are moderate in comparison to those of the S states (see Table III) but are of particular interest since their on-shell (phase shift) results are quite different as are the f ratios for each of the interactions as displayed in Figs. 1 and 3 respectively. The off-shell structure reflects the variations in the on-shell and half-on-shell results. All interactions display an initial, low momentum, peak followed by a ridge along the diagonal in the real part. The low momentum peak is more pronounced in the Reid and our t matrices than in the Paris

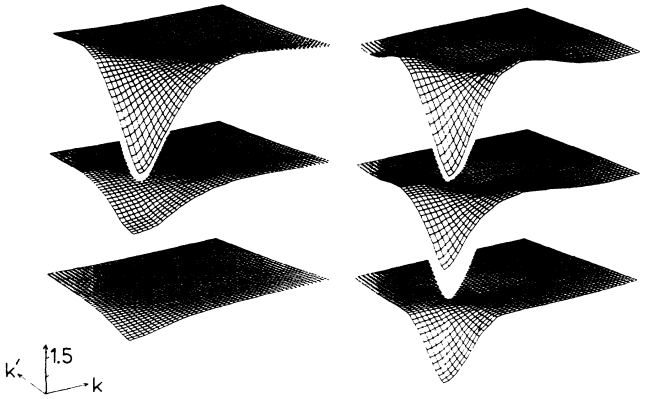

FIG. 13. As for Fig. 8 but for the type $n=0$, imaginary parts of the $^3S_1$ t matrices.

interaction results. With our interaction the ridge has more sharply defined structure on a surrounding depressed (and negative) valley arising from the q^2 dependence of our interaction. Such is not the case with either the Reid or the Paris t matrices as the former is but a sum of Yukawa functions whilst the latter has an energy dependent term which produces the growing $k=k'$ ridge.

The 0.5 MeV imaginary terms are not shown in Fig. 10 as for all interactions the values, even with $n=-1$, are very small. At 50 and 200 MeV the imaginary $^1P_1$ t matrix basically has the form of a well with the Paris values remaining relatively unchanged with energy. The Reid and our t matrices have deeper wells in the structure of the imaginary parts as energy is increased but, in addition, our t matrix also gains a stronger positive variation in the higher momenta. From this the nodal line relationship associated with unitarity is quite evident and cross correlates with the $^1P_1$ f ratios given in Fig. 3. The nodal line in the imaginary t matrix from our interaction occurs at 3.8 fm^{-1} at which momentum our $^1P_1$ f ratio changes sign.

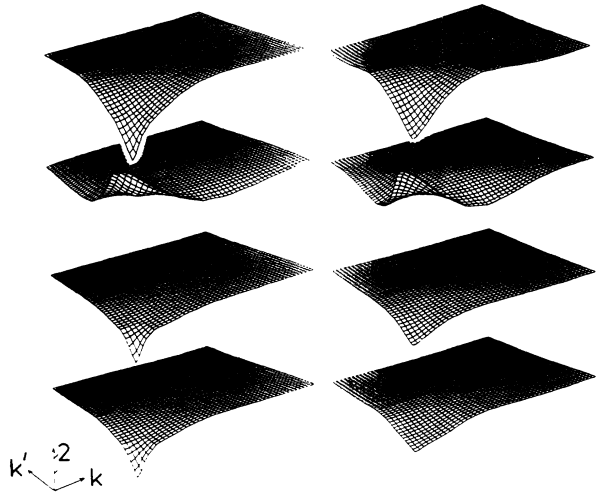

FIG. 12. As for Fig. 7 but for the real parts of the $^3S_1$ t matrices.

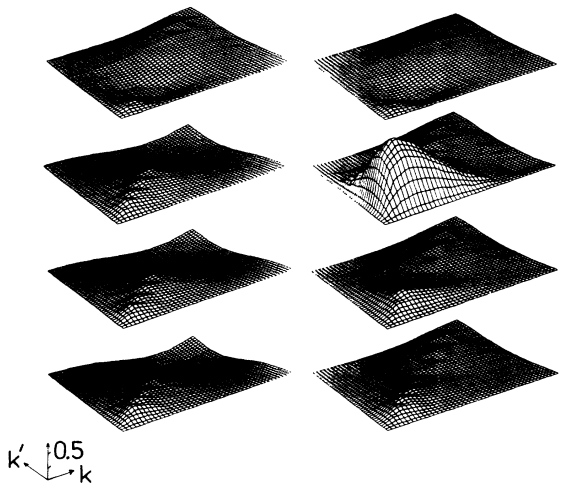

FIG. 14. As for Fig. 7 but for the real parts of the $^3D_1$ t matrices.

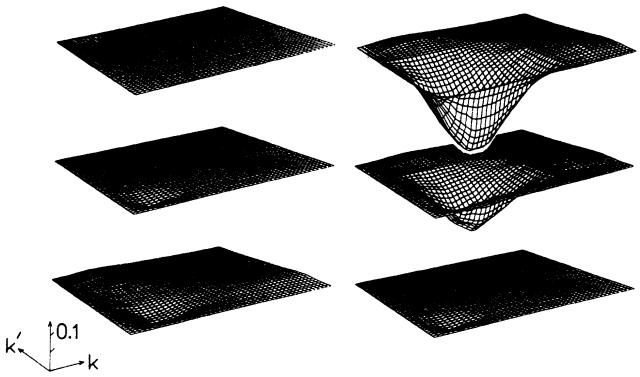

FIG. 15. As for Fig. 8 but for the type $n=0$, imaginary parts of the $^3D_1$ t matrices.

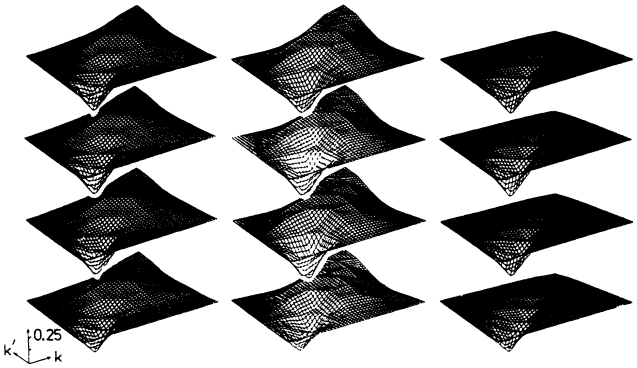

FIG. 17. As for Fig. 9 but for the real parts of the $^3D_2$ t matrices.

Such unitarity nodal line character is even more evident in the $^3P_0$ t matrix shown in Fig. 11 which contains the real and imaginary parts of our t matrix. The Paris and Reid results are very similar to our t matrix in this case and are not shown although the Reid values tend to be softer at high momenta. Such similarity follows those of the fits to the phase shifts (Fig. 1) and those of the half-on-shell f ratios (Fig. 4). The real part of our t matrix in this case has a small attractive well at small momenta and a repulsive ridge along the diagonal $k=k'$. The real part of the $^3P_0$ t matrix is quite energy independent. That is not the case with the imaginary part which varies from a mere depression at 0.5 MeV, to the diagonal symmetric well and peak form at 50 MeV and to a large well at 200 MeV. At the intermediate energy, the nodal line result of the unitarity condition is most evident at about 1.6 fm^{-1} at which value the half-on-shell f ratios of all three forces have their zero value.

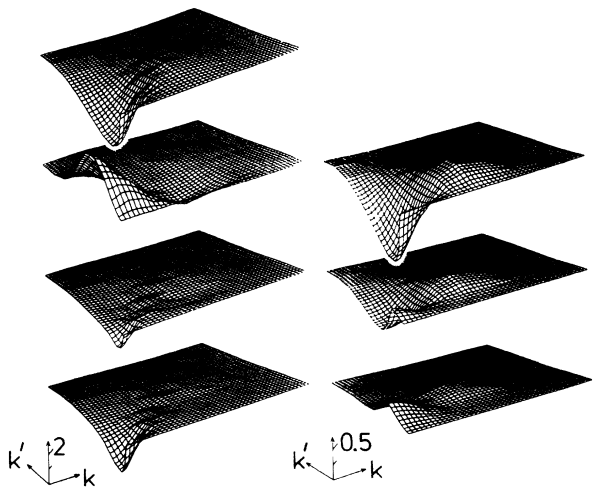

FIG. 16. The off-diagonal, $^3S_1$-$^3D_1$ t matrices (real parts in the left-hand panel, imaginary parts in the right-hand panel) for the common energy sequence.

We consider next the t matrices for the $^3S_1$, $^3D_1$, and the off-diagonal $^3S_1$-$^3D_1$ channels. Thereby we anticipate some reflection of a tensor force in each interaction case. This should be most evident in the diagonal $^3D_1$ and off-diagonal $^3S_1$-$^3D_1$ cases since the $^3S_1$ results (phase shifts) have very strong contributions from central forces and to first approximation the tensor coupling effects are masked. The $^3D_1$ (and ϵ_1) phase shifts are not so dominated by other interaction component effects. The f ratios for these channels vary markedly with the interactions and that has already been interpreted as evidence of a much weaker (off-shell) tensor force attribute of our interaction in comparison to either the Paris or the Reid cases.

The $^3S_1$ t matrices from our and the Paris interactions (the Reid is very similar) are shown in Figs. 12 and 13 for the real and imaginary parts (type $n=0$), respectively. The real parts of this t matrix show a marked variation with energy having a low momentum repulsive structure for ω at 0.5 MeV. This variation coincides with the (on-shell) phase shift passing through 90°; the only channel in which this occurs. Our interaction gives a sharper variation with momenta in the real part of these t matrices than is the case of the Paris interaction and this is particularly noticeable at the higher energies. The imaginary terms on the other hand vary simply with energy and the Paris interaction results vary more sharply with momentum at all energies, ω. At 200 MeV (400 MeV in the lab frame) the t matrix from our interaction is essentially purely real. This reflects the fact that at

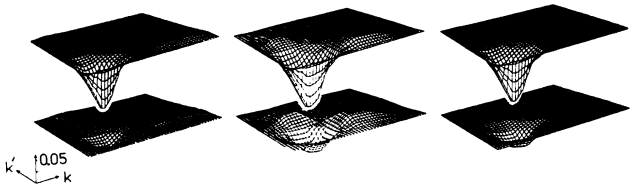

FIG. 18. As for Fig. 10 but for the type $n=-1$, imaginary parts of the $^3D_2$ t matrices.

TABLE III. The off-shell t matrix scalings.

State	Real Low	Real High	n	Imag. Low	Imag. High
$^1S_0$	−4.40	1.70	1	−0.70	0.30
$^1P_1$	−0.17	0.34	−1	−0.12	0.03
$^3P_0$	−0.4	0.5	−1	−0.07	0.04
$^3S_1$	−5.00	4.20	0	−2.70	0.90
$^3D_1$	−0.37	1.32	0	−0.53	0.04
$^3S_1$-$^3D_1$	−1.30	1.90	0	−1.20	0.40
$^3D_2$	−0.37	0.30	−1	−0.10	0.02

this energy our calculated phase shift in this channel is zero. The null phase shift value occurs with the Paris interaction at a lower energy.

The $^3D_1$ results are shown in Figs. 1, 4, and 15 for the real and imaginary (type $n=0$) parts. The Reid and Paris interaction are again very similar as one may anticipate from their comparable on-shell (phase shift) variation (to 400 MeV) and f ratios. The t matrix in this channel is small in magnitude in all cases. Our interaction t-matrix values vary little with energy and have very small imaginary values at all energies. The Paris interaction t matrix has a behavior at 50 and 200 MeV that is similar to our interaction results although the imaginary values are more pronounced. But the biggest variation occurs in the t matrix at low energies. For ω at 0.5 MeV the Paris interaction produces a t matrix that has a prominent peak (well) in the real (imaginary) part of the t matrix.

An even more dramatic variation of the Paris t matrix with energy and in comparison to that obtained using our interaction, is found in the off-diagonal $^3S_1$-$^3D_1$ results. The real and imaginary parts of the t matrix we have obtained by using the Paris interaction are displayed in Fig. 16. The t matrix obtained using our interaction is so small in comparison that it is not depicted. Being off diagonal the t matrix is not symmetric about the $k=k'$ diagonal. However, there is a symmetry with the $^3D_1$-$^3S_1$ off-diagonal matrix which is a reflection across the diagonal of the results displayed in Fig. 16. The strong variation at low energies as observed in the (diagonal) $^3D_1$ results is again present.

In this coupled channel, there were sizable differences (on shell) in predictions of ϵ_1 found using our interaction and the Paris interaction. Such differences are even more dramatic in the off-shell behavior of the respective t matrices.

The $^3D_2$ phase shifts as shown in Fig. 1 given by the three interactions are quite different at the higher energy region and so we consider the off-shell properties of this channel to complete this study. The real and imaginary parts (type $n=-1$) of the $^3D_2$ t matrices are displayed in Figs. 17 and 18, respectively, with the low energy ($\omega=0.5$) imaginary values omitted since they are very small at all momenta. The real parts of the Reid t matrix appear as a sequence of wells along the diagonal at all energies while those of our and the Paris interaction have a developed ridge at higher momenta. The imaginary parts have similar single well form with a similar energy variation but our interaction gives higher momentum rises that are even more accentuated in the Paris interaction results. The nodal lines due to unitarity are again evident and particularly so for the Paris results.

Our results are confirmed by the recent study of the $K(R)$-matrix structures obtained from the Reid and Paris interactions[17] and which was confined to the energy range 50 to 350 MeV (lab). That study revealed a number of distinctive features of the associated t matrices, all of which we have observed in our study. In particular the marked variation of the $^1P_1$ channel results has been reproduced.

But by our analysis of lower energy cases we have also found aspects of the t matrix that could not be anticipated from the previous work.[17] We have also portrayed properties of the t matrix at higher momentum values; albeit that such may be a regime in which the very concept of a t matrix may be inappropriate.

VII. COMPUTATIONAL ASPECTS OF t-MATRIX SOLUTION

As stated previously, we have calculated the off-shell t-matrix elements using two distinctly different methods, namely matrix inversion and the method of continued fractions. For the matrix inversion calculation one must use a high accuracy matrix inversion routine, even to obtain the on-shell elements (phase shifts). The subroutine we used in our computation was taken from the IMSL library, and featured iterative refinement. The time taken to calculate the off-shell matrix elements by matrix inversion scales uniformly as N^2, the square of the number of grid points ($4N^2$ for the coupled states). Typically, each uncoupled state can be solved in 1 sec if one uses 15 Gauss-Laguerre points on a VAX 8650 (VMS 4.4) system. But to attain an accuracy of one part in 10^3 for all k,k' of interest, this matrix inversion scheme should use at least 25 Gauss-Legendre points. We note that for the same scheme and accuracy, 15 Gauss-Laguerre points suffice for most channels. But we also note that the low energy properties of the t matrix from which scattering lengths and the deuteron properties can be deduced need at least 32 Gauss-Laguerre point evaluations to obtain convergence with the necessary accuracy.

Using the continued fraction method required similar operation times to achieve the same overall accuracy of one part in 10^3. For uncoupled channels the computational times with this method give little or no saving upon those required by the matrix inversion method. However, for the coupled channels, and if larger N is to be used, then considerable saving is possible using this method.

VIII. SUMMARY

The primary purpose of our study has been to delineate essential features of the (complex) t matrix of the free two nucleon problem. To achieve this we have com-

pared the t matrices found using model interactions that give reasonable to good fits to on-shell phase shift data but which are rather different in their functional form. Specifically we have used the phenomenological interaction of Reid, the derived interaction of the Paris group, and a new phenomenological interaction that we have specified by obtaining good fits to the elastic scattering phase shifts up to a laboratory energy of 400 MeV and the properties of the deuteron. Our interaction has the twin advantages of a simple form factor prescription involving but three ranges and of a form that facilitates calculations. With our chosen mass scalings the component interaction strengths required to fit data in all channels are very simple, often integer, numbers and are ones which are quite characteristic of expectation values of simple operators.

The properties of our interaction have been compared with those of the standard interaction models of Reid and of the Paris group. All gave good to excellent fits to the on-shell phase shift data below 400 MeV for the $^1S_0$, $^3S_1$, $^3P_0$, and $^3P_1$ states in particular. They were also notable for their quite diverse predictions of phase shifts in the $^1P_1$ and $^3D_2$ states and the coupling parameter ϵ_1, especially. Such behavior is reflected even more strongly in the off-shell t matrices.

The close similarity of all interactions off-shell properties in those channels in which they all agree on shell, in view of their disparate interaction form factors, suggests that the actual t matrix in those channels are insensitive to exactly which model form of interaction is chosen provided that the interaction gives a good on-shell (phase shift) fit over a reasonable energy range. Accepting that suggestion, and as our interaction was chosen specifically to provide good fits to the on-shell data, then our off-shell t matrix so deduced for channels such as the $^1P_1$ and $^3D_2$, etc. would be suitable for use in relevant calculations. So different are they from the Paris and Reid values that the nuclear reaction data whose analyses would sample those t-matrix properties would confirm or deny our suggestions.

This research was supported by grants from the Australian Research Grants Scheme and from the Fondo Nacional de Desarrollo Cientifico y Tecnologico, Chile.

---

*Permanent address: Departamento de Fisica, Casilla 487/3, Universidad de Chile, Santiago, Chile.

†Permanent address: Bureau of Meteorology Research Centre, G.P.O. Box 1289K, Melbourne, Australia.

[1]A. Kerman, H. McManus, and R. M. Thaler, Ann. Phys. (N.Y.) **8**, 551 (1959); S. J. Wallace in *Advances in Nuclear Physics*, edited by J. Negele and E. Vogt (Plenum, New York, 1981), Vol. 12; L. Ray, Phys. Rev. C **19**, 1855 (1979); **20**, 1857 (1979).

[2]F. A. Brieva and J. R. Rook, Nucl. Phys. **A291**, 219, 317 (1977).

[3]H. V. von Geramb, L. Rikus, and K. Nakano, in Proceedings of the RNCP International Symposium on Light Ion reaction Mechanics, 1983, Osaka, Japan.

[4]M. Lacombe, B. Loiseau, J. M. Richard, R. Vinh Mau, J. Côté, P. Pirès, and R. de Tourreil, Phys. Rev. C **21**, 861 (1980).

[5]L. Rikus, K. Nakano, and H. V. von Geramb, Nucl. Phys. **A414**, 413 (1984).

[6]T. Hamada and I. D. Johnston, Nucl. Phys. **34**, 382 (1962).

[7]R. V. Reid, Ann. Phys. (N.Y.) **50**, 411 (1968).

[8]K. Erkelenz, Phys. Rep. **13C**, 191 (1974); K. Holinde, *ibid.* **68**, 121 (1981).

[9]B. L. G. Bakker, M. Bozoian, J. N. Maslow, and H. J. Weber, Phys. Rev. C **25**, 1134 (1982); A. Faessler, Prog. Part. Nucl. Phys. **11**, 171 (1984); M. Beyer and H. J. Weber, Phys. Rev. C **35**, 14 (1987).

[10]L. Petris, J. Phys. **G7**, 309 (1981); L. Berge and L. Petris, Aust. J. Phys. **39**, 461 (1986).

[11]M. I. Haftel and F. Tabakin, Nucl. Phys. **A158**, 1 (1970).

[12]H. Horáček and T. Sasakawa, Phys. Rev. A **30**, 2274 (1984); Phys. Rev. C **32**, 70 (1985).

[13]M. Abramowitz and I. Stegun, *Handbook of Mathematical Functions*, No. 55 Natl. Bur. Stand. (U.S.) Applied Mathematical Series, edited by M. Abramowitz and I. Stegun (U.S. GPO, Washington, D.C., 1964).

[14]R. A. Arndt, L. D. Roper, R. A. Bryan, R. B. Clark, B. J. Ver West, and P. Signell, Phys. Rev. D **28**, 97 (1983); R. A. Arndt, J. S. Hyslop III, and L. D. Roper, *ibid.* **35**, 128 (1987).

[15]G. E. Brown and A. D. Jackson, in *The Nucleon-Nucleon Interaction* (North-Holland, Amsterdam, 1976), p. 74.

[16]P. D. B. Collins and A. D. Martin, in *Hadron Interactions* (University of Sussex, Sussex, 1984); G. Giacomelli, Phys. Rep. **23**, 123 (1976); K. Gadianos, *ibid.* **101**, 170 (1983).

[17]E. F. Redish and K. Stricker-Bauer, Phys. Rev. C **36**, 1183 (1987).

[18]S. K. Adhikar and L. Tomio, Phys. Rev. C **33**, 467 (1986).

[19]L. Tomio and S. K. Adhikar, Phys. Rev. C **22**, 28 (1980).

[20]H. P. Noyes, Phys. Rev. Lett. **15**, 538 (1965); K. L. Kowalski, *ibid.* **15**, 798 (1965).

[21]J. Haidenbauer, Y. Koike, and W. Plessas, Phys. Rev. C **33**, 439 (1986); K. Schwarz, J. Haidenbauer, and J. Frohlich, *ibid.* **33**, 456 (1986).

[22]J. J. DeSwart and M. M. Nagels, Forstchr. Phys. **28**, 215 (1978).

[23]R. M. Woloshyn and A. D. Jackson, Nucl. Phys. **A185**, 131 (1972).

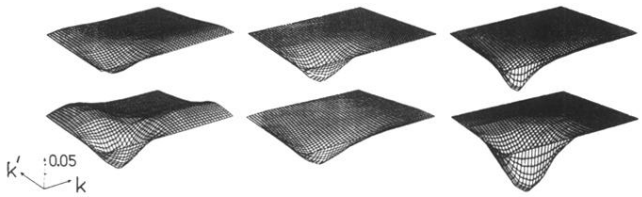

FIG. 10. The imaginary (type $n = -1$) $^1P_1$ channel t matrices from our, Paris and Reid interactions (left to right) and at energies of 50 and 200 MeV (top to bottom).

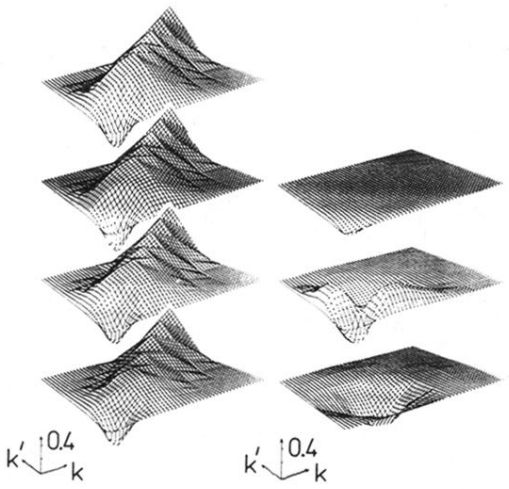

FIG. 11. The $^3P_0$ t matrices obtained using our interaction. The real parts are for energies -50, 0.5, 50, and 200 MeV are shown from top to bottom in the left-hand panel. The imaginary (type $n=-1$) parts for the positive energy sequence are shown on the right.

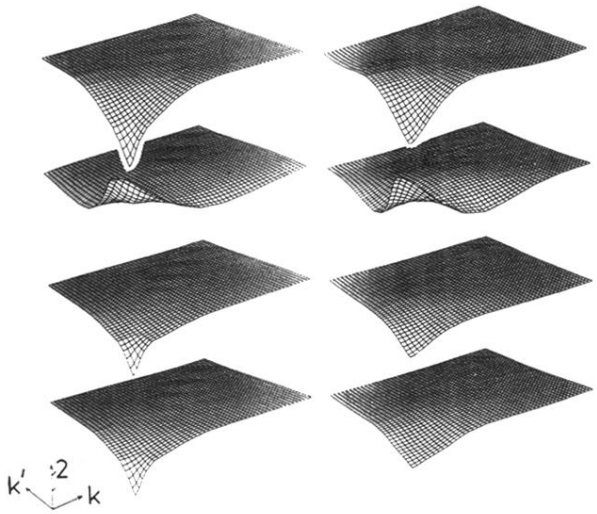

FIG. 12. As for Fig. 7 but for the real parts of the $^3S_1$ t matrices.

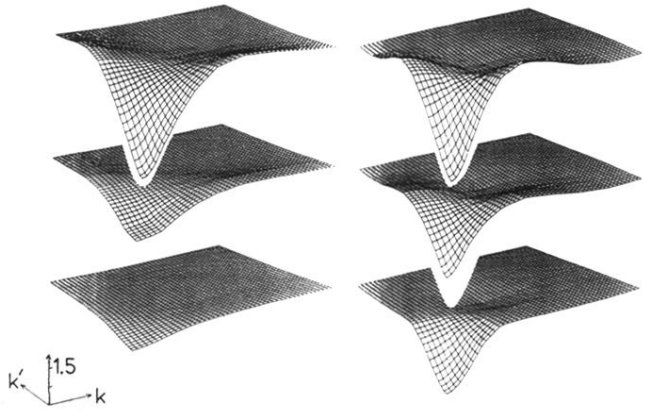

FIG. 13. As for Fig. 8 but for the type $n=0$, imaginary parts of the ${}^3S_1$ t matrices.

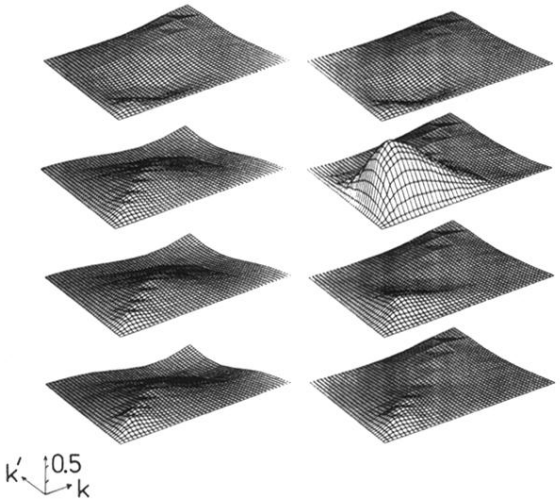

FIG. 14. As for Fig. 7 but for the real parts of the ${}^3D_1$ t matrices.

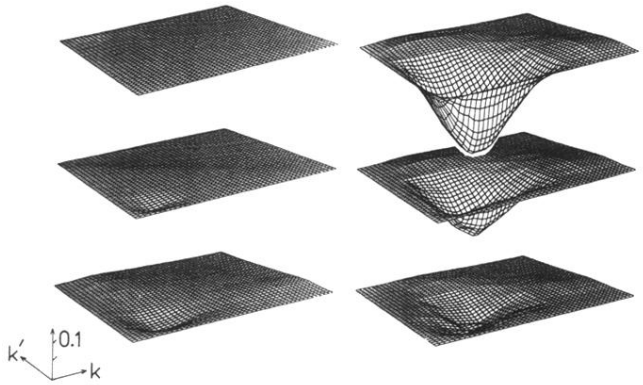

FIG. 15. As for Fig. 8 but for the type $n=0$, imaginary parts of the ${}^3D_1$ t matrices.

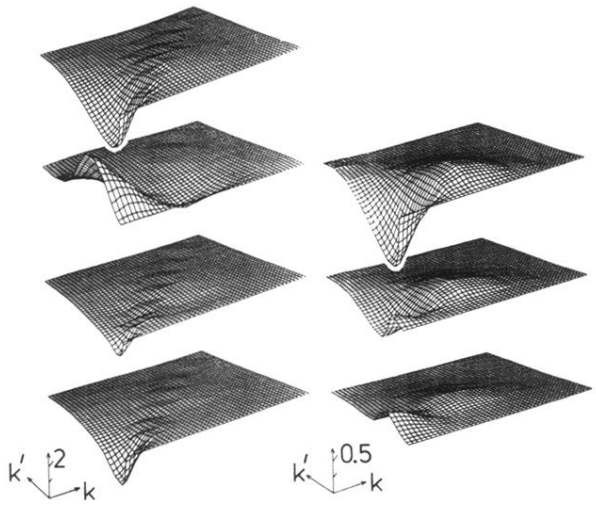

FIG. 16. The off-diagonal, $^3S_1$-$^3D_1$ t matrices (real parts in the left-hand panel, imaginary parts in the right-hand panel) for the common energy sequence.

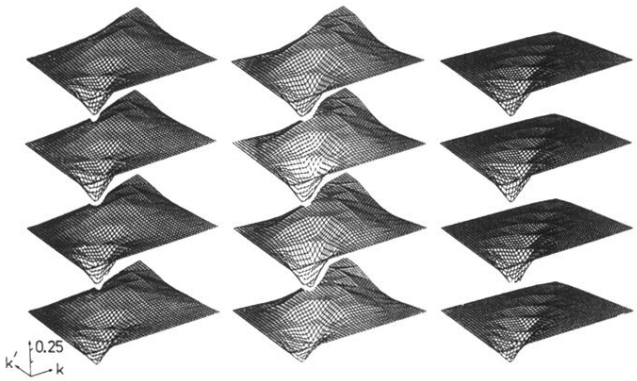

FIG. 17. As for Fig. 9 but for the real parts of the $^3D_2$ t matrices.

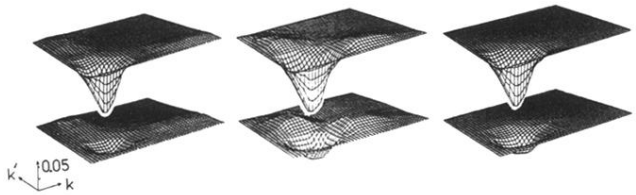

FIG. 18. As for Fig. 10 but for the type $n = -1$, imaginary parts of the ${}^3D_2$ t matrices.

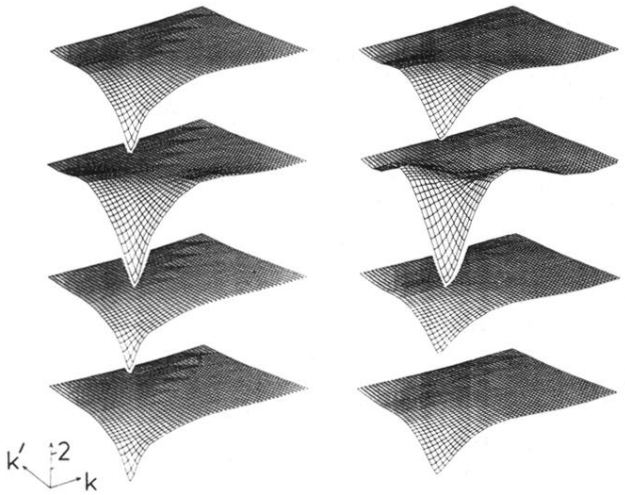

FIG. 7. The real parts of the Paris (right panel) and our (left panel) interaction t matrices in the $^1S_0$ channel. From top to bottom are shown the results found using a center of mass energy (ω) of -50.0, 0.5, 50.0, and 200.0 MeV.

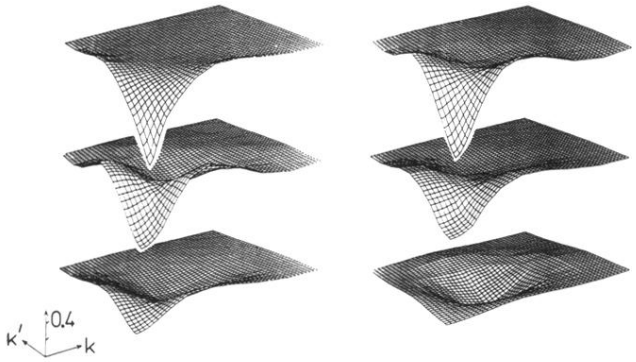

FIG. 8. The $n=1$ type imaginary parts of the ${}^1S_0$ t matrices relevant to the positive energy parts of Fig. 7.

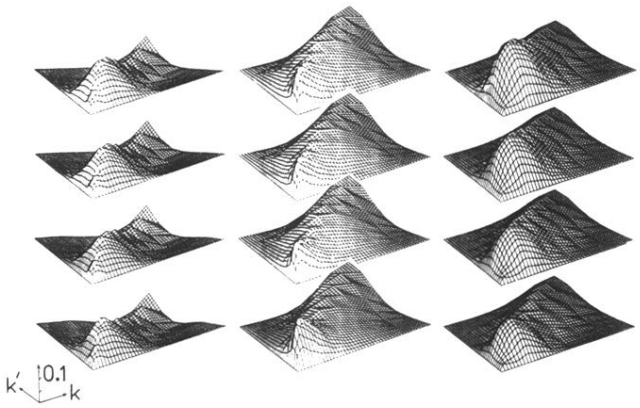

FIG. 9. The real parts of the Reid (right panel), Paris (center panel), and our interaction (left panel) t matrices in the $^1P_1$ channel for the sequence of center of mass energies used in Fig. 7.